EFFECTS OF CHLORIDE ON COPPER CORROSION AND CATHODIC CHARGING OF CARBON STEEL FOR NUCLEAR WASTE DISPOSAL APPLICATION

Prepared for

U.S. Nuclear Regulatory Commission
Contract NRC–HQ–12–C–02–0089

Prepared by

Xihua He[1]
Tae Ahn[2]

[1]Center for Nuclear Waste Regulatory Analyses
San Antonio, Texas

[2]U.S. Nuclear Regulatory Commission
Washington, DC

September 2017

ABSTRACT

Copper (Cu) and carbon steel are candidate waste container materials for high-level radioactive waste geologic disposal systems located in the saturated zone. This study investigated the role of chloride (Cl^-) in Cu corrosion in anaerobic solutions containing sulfate (SO_4^{2-}) and Cl^-, which are dominant anions in groundwater. SO_4^{2-} concentration was kept constant at 2×10^3 ppm, while Cl^- concentration was varied from 0 to 1×10^3, 1×10^4, and 1×10^5 ppm. The corrosion potential decreased with increasing Cl^- concentration, leading to potentially larger corrosion tendency. Increasing Cl^- concentration from 0, to 1×10^3 ppm, and to 1×10^4 ppm led to an increase in the corrosion rate. The rate in the solution with 1×10^5 ppm Cl^- was lower than in the 1×10^3 ppm solution. However, all the corrosion rates measured at ambient temperature were below 10 nm/yr [4×10^{-7} in/yr], which was 1 to 2 orders of magnitude lower than what was measured previously in simulated granitic groundwater at 50 °C [122 °F]. Overall, the electrochemical data showed that corrosion tendency was negligible in SO_4^{2-}-only solution and increased with increasing Cl^- concentration over the concentration range in this work. Tests at elevated temperatures are needed to further investigate the roles of Cl^- and other species such as bicarbonate on copper corrosion.

This study also investigated the hydrogen induced cracking (HIC) tendency of carbon steel under cathodic charging in simulated concrete pore water. A cathodic charging current of 0.5 mA/cm^2 [3.2 mA/in^2] was applied to the apex of a U-bend. The tests were conducted at 50 °C [122 °F] for a duration of 1.5 to 3 months. The potential needed for the current was in the range of −1.3 to −1.2 V_{SCE} for the first 50 days, but it fluctuated to more negative values later on. In two of the three tests, 100 ppm Cl^- and 100 ppm S^{2-} were added to the $Ca(OH)_2$ solution. Under the given time and test conditions, the A516 Grade 60 carbon steel material used in this work is highly resistant to hydrogen induced cracking because (i) the alkaline solution forms a passive scale on the surface, leading to low hydrogen absorption efficiency and (ii) the short-term static stress from the U-bend is not in the range that would render cracking susceptibility. The HIC degradation mechanism for carbon steel material in disposal applications will need to be evaluated further under other test conditions, such as in neutral granitic solution.

CONTENTS

FIGURES

TABLES

ACKNOWLEDGMENTS

QUALITY OF DATA, ANALYSES, AND CODE DEVELOPMENT

DATA: All CNWRA-generated original data contained in this report meet the quality assurance requirements described in the CNWRA Quality Assurance Manual. Sources for other data should be consulted for determining the level of quality for those data. Scientific Notebook 1312 was used (He, 2017) to document the experimental conditions and in-process entries.

ANALYSES AND CODES: none

REFERENCES:

He. X. "Copper and Carbon Steel Experiments." Scientific Notebook 1312. San Antonio, Texas: Center for Nuclear Waste Regulatory Analyses. pp. 1–28. 2017.

1 INTRODUCTION

Many countries have been exploring the feasibility of high-level waste (HLW) disposal in deep geologic repositories. The groundwaters in these repositories may contain a very low level of oxygen and copper (Cu) is a candidate container metal because it corrodes very slowly in such environments. Cu has been proposed for use as a waste package material in a number of high-level radioactive waste repository programs, including those in Switzerland, Sweden, Finland, Japan, and Canada (King, 2013). Carbon steel is being considered in different ways as a candidate material for waste packages in HLW geologic disposal systems in several countries (Martin et al., 2014; Kursten et al., 2011; Shibata et al., 2014; King et al., 2014; Boyle and Meguid, 2015). In the Belgian supercontainer concept, the carbon steel overpack is surrounded by a thick concrete buffer (Kursten et al., 2011). Some nations, such as Canada, looking at Cu-coated steel packages propose to use steel as an internal structural material where steel is not in direct contact with solution (Boyle and Meguid, 2015).

This report continues the independent analyses of Cu and carbon steel waste container materials previously reported in He et al. (2015), He and Ahn (2017), and He et al. (2018). Cu corrosion tests were conducted in anaerobic solutions containing common species, such as sodium (Na^+), calcium (Ca^{2+}), chloride (Cl^-), and sulfate (SO_4^{2-}), found in most deep groundwaters. Similar to the previous tests, experimental studies for carbon steel were conducted in reducing alkaline solutions to simulate an environment in the presence of a concrete overpack. The specific objectives of this work were to

- Evaluate effects of Cl^- concentration

- Assess carbon steel hydrogen-induced cracking (HIC) tendency under cathodic charging

This report is organized into four chapters. Chapter 1 is an introduction, Chapter 2 describes the experimental approaches, Chapter 3 presents the data on copper and carbon steel corrosion, and Chapter 4 presents a summary.

2   EXPERIMENTAL APPROACHES

The Cu and carbon steel tests were conducted in (i) SO_4^{2-} and Cl^- solutions and (ii) concrete pore water, respectively. All the tests were designed to establish an anaerobic environment by removing oxygen (O_2) from the solution and preventing air entry into the solution.

2.1   Copper Corrosion Tests in Solution with Varying Chloride Concentration

In most deep groundwaters, Cl^- is the dominant anion, with SO_4^{2-} also present in significant concentrations for some host rock types. Na^+ and Ca^{2+} tend to be the predominant cations (King, 2013). Because of the presence of these dominant species and the objective to investigate the role of Cl^- on copper corrosion, tests were conducted in solutions with SO_4^{2-} and Cl^- as the only anions. SO_4^{2-} concentration was kept constant at 2×10^3 ppm by adding sodium sulfate (Na_2SO_4). Cl^- concentration was varied from 0 to 1×10^3, 1×10^4, and 1×10^5 ppm by adding a constant amount of calcium chloride ($CaCl_2$), except for the zero Cl^- solution, and a varying amount of sodium chloride (NaCl). Tests were conducted in anaerobic conditions in a glovebox purged with nitrogen (N_2) at ambient temperature {about 20 °C [68 °F]}. The O_2 concentration in the glovebox was calibrated and monitored, and was usually in the range of 3–6 ppm. Based on a Henry's constant of 1.3×10^{-3} mol/(L·atm), the O_2 concentration in solution was about 0.1–0.2 ppb.

The test matrix is shown in Table 1. Oxygen-free high conductivity copper cylindrical electrodes, which are the same as those used in our previous work (He at al., 2015; He and Ahn, 2017), were used in the tests. Open circuit potential (E_{OC}) was monitored and electrochemical impedance spectroscopy (EIS) was performed after several days of E_{OC} monitoring. For the four tests shown in Table 1, total test duration ranged from 14 to 22 days. EIS measurements were performed using a Gamry potentiostat. The validity of impedance data was checked using the Kramers–Kronig transform. All measurements were performed with the potential held at the value of E_{OC} using a perturbation voltage signal of 10 mV (rms) applied over the frequency range from 10^5 to 10^{-3} Hz. Ten data points per decade were recorded. Electrochemical impedance is the response of an electrochemical system to an applied potential. The frequency dependence of this impedance can reveal underlying chemical processes. The complex response of the system is usually displayed in Nyquist format and Bode plot. The capacitance at the metal/electrolyte interface always plays an important role. Details about EIS are described in the Appendix.

On completion of the experiments, the Cu electrodes were analyzed by scanning electron microscope (SEM) and Energy Dispersive X-Ray Spectroscopy (EDX).

2.2   Cathodic Charging of Carbon Steel in Simulated Concrete Pore Water

The carbon steel materials and the simulated concrete pore water were the same as those used in previous work (He at al., 2015; He and Ahn, 2017). An alkaline solution prepared from saturated $Ca(OH)_2$ without adjustment of pH was used to simulate concrete pore water. The solution was deaerated with N_2 gas to achieve an anaerobic condition. Cathodic charging tests were conducted on carbon steel single U-bends. The test matrix is shown in Table 2. The cathodic charging current was about 0.5 mA/cm^2 [3.2 mA/in^2]. To have a controllable surface area and to have the stressed region charged, the two legs of the U-bends were embedded in epoxy, leaving only the apex of the U-bend exposed in solution. In two of the three tests, 100 ppm Cl^- and 100 ppm sulfide (S^{2-}) were added to the tests. All the tests were conducted at 50 °C [122 °F].

Table 1. Test matrix on evaluating effects of chloride on Cu corrosion						
Cell	Solution #	Na_2SO_4 (mol/L)	$CaCl_2$ (mol/L)	NaCl (mol/L)	T, °C	Methods
Glass cell set up in anaerobic glovebox	1	0.02*	0	0	20†	Open circuit potential and electrochemical impedance spectroscopy
	2	0.02	0.01	0.008	20	
	3	0.02	0.01	0.26	20	
	4	0.02	0.01	2.8	20	

*This concentration makes 2,000 ppm SO_4^{2-}.
Solution 1: [Cl^-] = 0
Solution 2: [Cl^-] = 1×10^3 ppm
Solution 3: [Cl^-] = 1×10^4 ppm
Solution 4: [Cl^-] = 1×10^5 ppm
†20 °C = 68 °F

Table 2. Test matrix on carbon steel cathodic charging				
Cell	Type of U-bends	Deaerated Solution	T, °C	Cathodic charging current
Glass cell	Single*	$Ca(OH)_2$	50†	0.5 mA/cm²
		$Ca(OH)_2$ + 100 ppm Cl^-	50	0.5 mA/cm²
		$Ca(OH)_2$ + 100 ppm S^{2-}	50	0.5 mA/cm²

*Only the apex of the U-bend was immersed in solution for cathodic charging
†50 °C = 122 °F

3 EXPERIMENTAL DATA AND RESULTS

3.1 Copper Corrosion Properties in Anaerobic Solution with Varying Chloride Concentration

The results described in this section correspond to the experiments described in Section 2.1.

3.1.1 Open Circuit Potential

Figure 1(a) shows the E_{OC} of Cu measured prior to each EIS measurement. The data are not continuous in some regions because of interruptions in the EIS measurement. After immersing the electrode in solution, the E_{OC} decreased with time at a faster rate at the beginning, but reached a steady state at a later time. It took only about 1 day for the E_{OC} to reach steady state in solutions with higher Cl^- concentrations. The steady state E_{OC} is plotted against Cl^- concentration in Figure 1(b), along with a data point in simulated granitic groundwater obtained previously at 50 °C [122 °F] (He and Ahn, 2017)—in which the solution contained a small amount of bicarbonate (HCO_3^-) in addition to Cl^- and SO_4^{2-}.

Corrosion of metals in aqueous environments occurs when one or more oxidation-reduction reactions take place simultaneously on a metal surface. For example, Cu dissolves or forms oxides or hydroxides driven by water reduction in an anaerobic neutral condition. The overall reaction can be expressed as:

$$2Cu + 2H_2O \Leftrightarrow 2CuOH + H_2 \tag{1}$$

where copper hydroxide (CuOH) is a simplified form of the corrosion products. Depending on the environmental conditions, the corrosion products could be more complex. The rate of corrosion can be expressed in terms of electrochemical current, which is known as the corrosion current, i_{corr}. During corrosion, the electrons liberated by the oxidation reaction are consumed by the reduction reaction. The total anodic current must be equal and opposite in sign to the total cathodic current. The potential at this condition is the corrosion potential, E_{corr}. This potential, measured against a reference electrode using a voltmeter or potentiostat with high input impedance, is the E_{OC}, where no current flows to or from the working electrode. Figure 2 illustrates schematically the Tafel approximation for the polarization curves (potential versus current density) in the form of E versus *log*i for both the cathodic and anodic reactions plotted on one graph; this plot is called an Evans diagram. The E_{OC} and i_{corr} can be obtained from the intersection of the two curves. Figure 1 shows that E_{OC} decreased clearly with increasing Cl^- concentration. This effect is illustrated in Figure 2, in which increasing Cl^- concentration shifts the anodic polarization curve in the more negative direction, resulting in a lower E_{OC} value and potentially larger i_{corr}. The potential role HCO_3^- plays in Cu corrosion is a potential topic for further investigation.

3.1.2 EIS

Figures 3, 4, 5, and 6 show the EIS data obtained from four solutions with varying chloride concentration at different times. The curves show the fits to the equivalent circuits used to represent the electrochemical system, which is described in the Appendix.
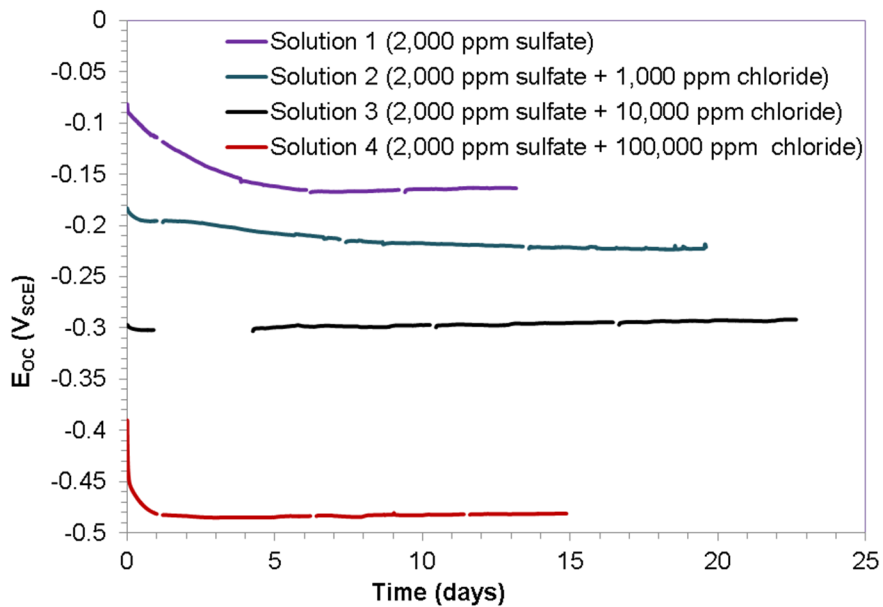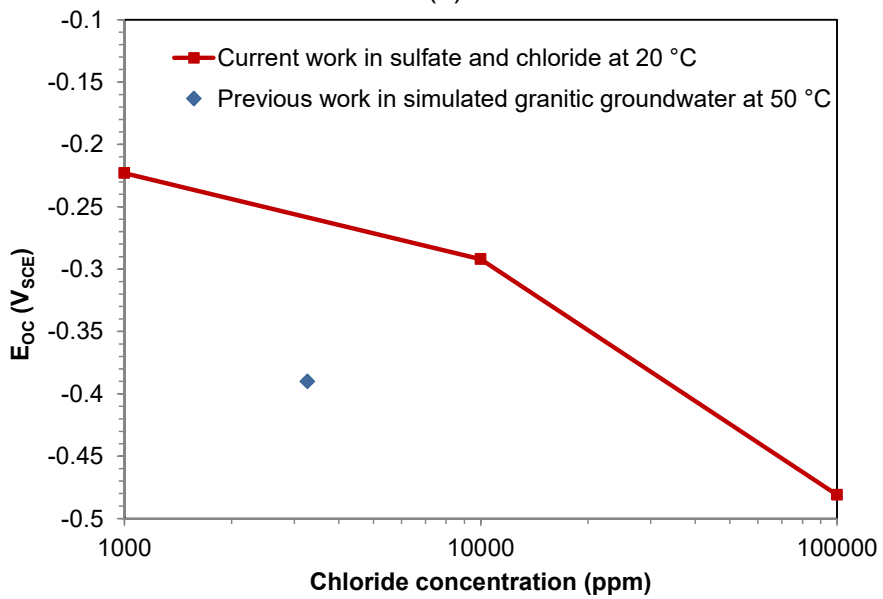
Figure 1. (a) E_{OC} of Cu as a function of time in 4 solutions with varying Cl⁻ concentration and (b) steady state E_{OC} as a function of Cl⁻ concentration along with one data point from previous work for comparison (He and Ahn, 2017)
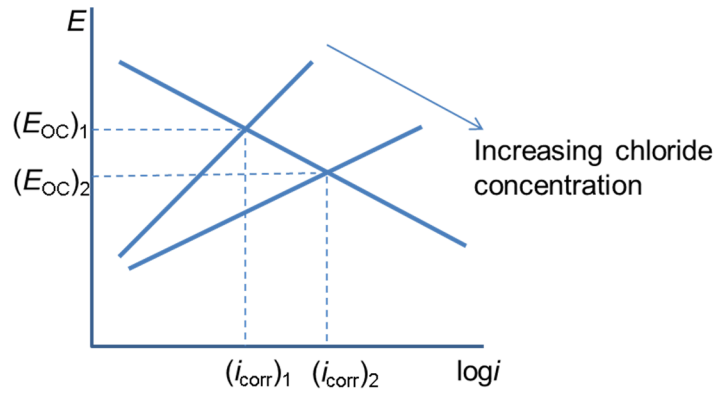
Figure 2. Effect of increasing Cl⁻ concentration on the E_OC and corrosion tendency
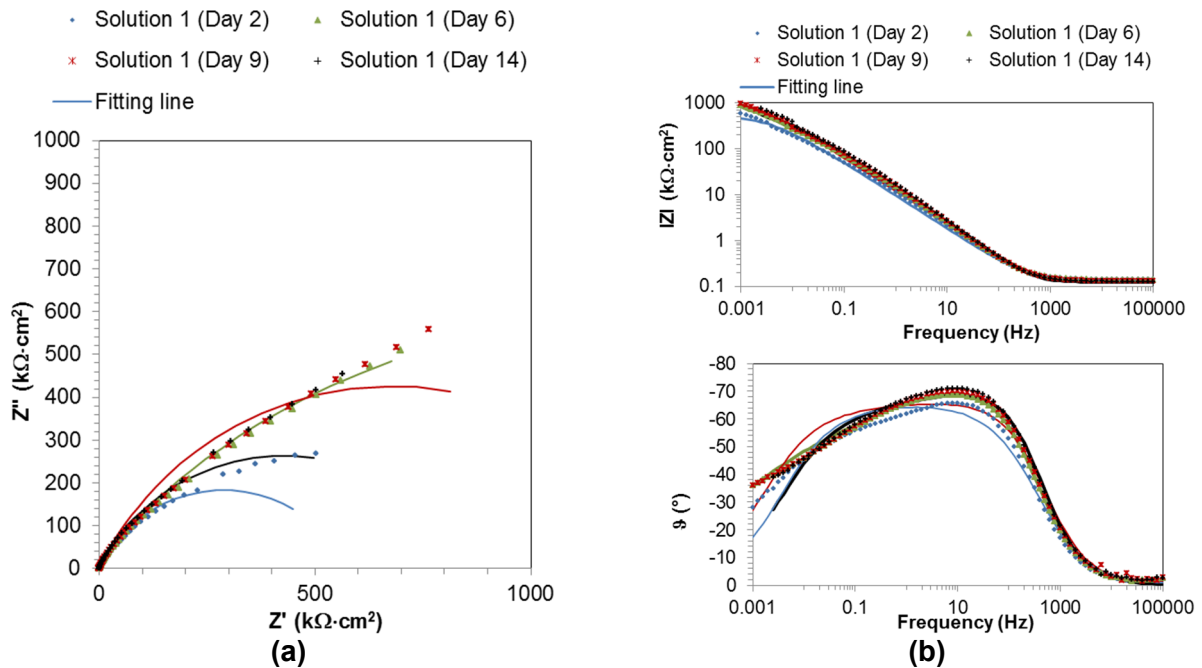
Figure 3. EIS of Cu exposed to Solution 1 (2,000 ppm SO_4^{2-}) at 2, 6, 9, and 14 days; (a) Nyquist plot and (b) Bode plot

6
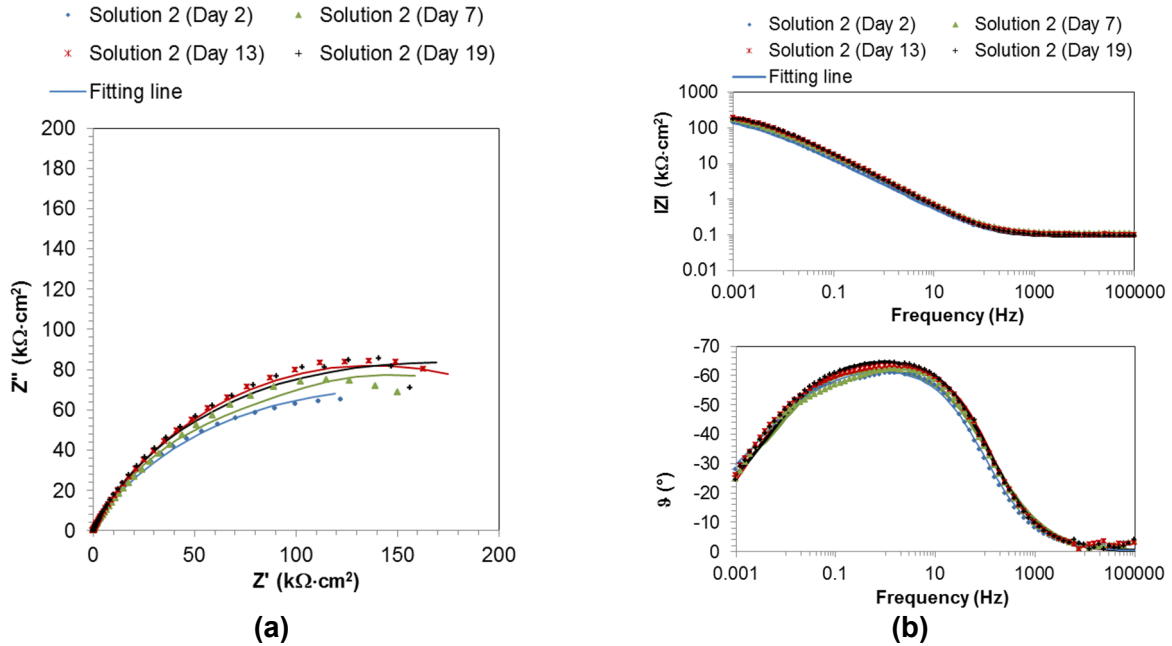
Figure 4. EIS of Cu exposed to Solution 2 (2,000 ppm SO_4^{2-} and 1,000 ppm Cl^-) at 2, 7, 13, and 19 days; (a) Nyquist plot and (b) Bode plot
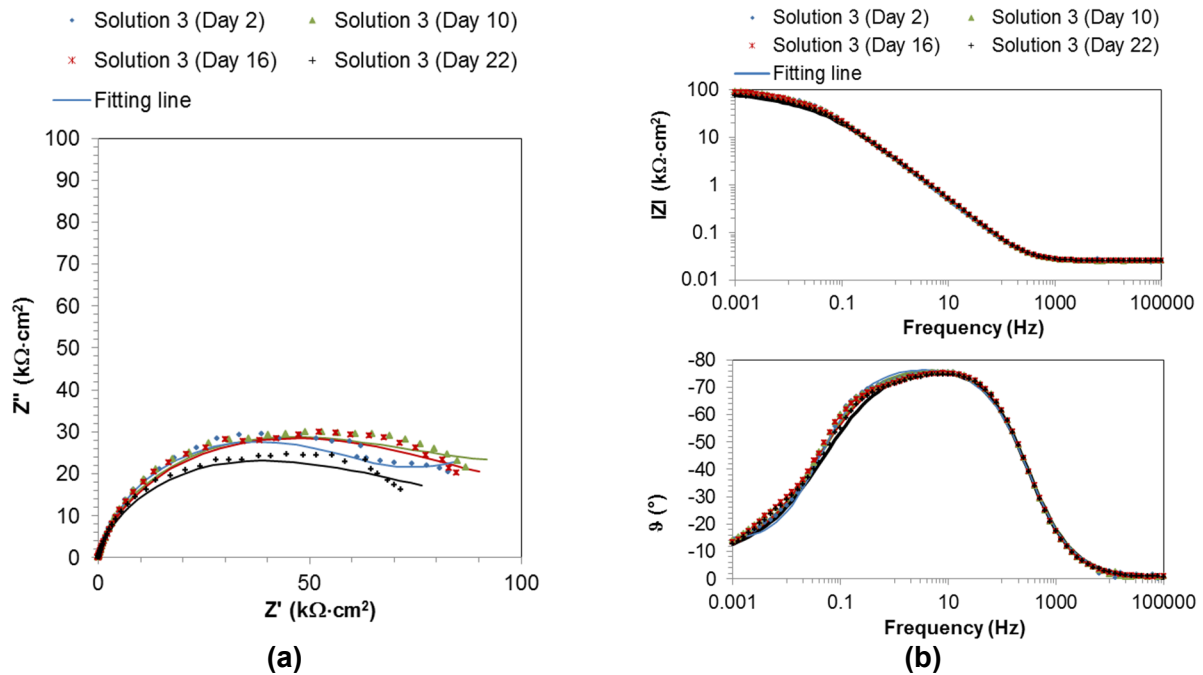
Figure 5. EIS of Cu exposed to Solution 3 (2,000 ppm SO_4^{2-} and 10,000 ppm Cl^-) at 2, 10, 16, and 22 days; (a) Nyquist plot and (b) Bode plot
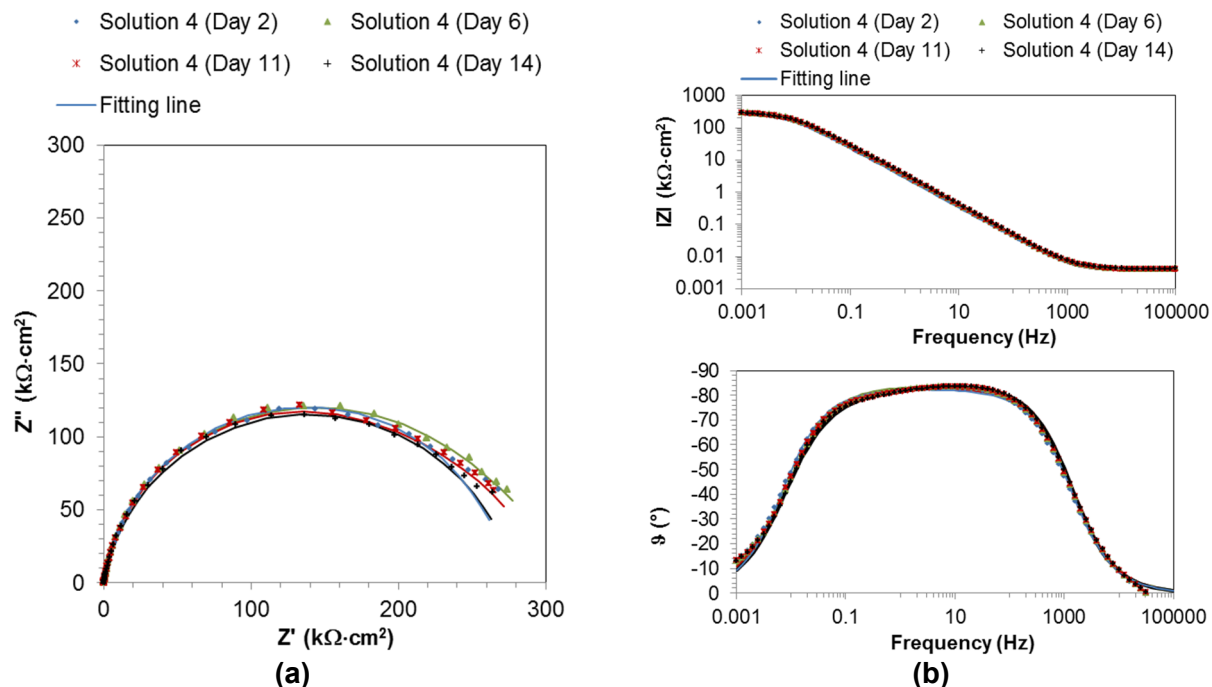
Figure 6. EIS of Cu exposed to Solution 3 (2,000 ppm SO$_4^{2-}$ and 100,000 ppm Cl$^-$) at 2, 6, 11, and 14 days; (a) Nyquist plot and (b) Bode plot

The data showed a mix of resistive and capacitive behavior and they do not change much with time over the test duration, suggesting that the environment was very stable in the glovebox. Diffusion is suggested in Figure 3(a), for the solution containing SO$_4^{2-}$ only, by a curve approximating a diagonal line with a slope of 45° in the Nyquist plot. The commonly accepted one time constant circuit used to model the electrochemical interface of a corroding metal [Figure 7(a)] was used first to model the EIS data, but the Nyquist plots and phase angle in the Bode plots in Figures 3 through 5 were not well represented by the model (not shown), especially in the low frequency region. The two-time constant circuit [Figure 7(b)], which is commonly used to model an inner barrier layer at the metal-solution electrochemical interface, was then used to fit the data. The curves on the EIS data plots are the fitting curves from the two-time constant circuit. The goodness of fit for Figures 3 through 5 improved slightly, but the Nyquist plot and phase angle in the Bode plot in Figure 3 still did not fit well with the model. This suggests that the data for Solution 1 (SO$_4^{2-}$ only) cannot be simply represented by the two models. Because all the amplitude data in the Bode plot were well represented by the one time constant circuit in Figure 7(a) and the rule-of-thumb is to choose the simplest and most basic model to represent the data if the more complex model gives the same level of confidence in representing the data, the results from the one time constant circuit model were analyzed further. The impedance of the equivalent circuit is desribed in Equation (A-7) in the Appendix.

The corrosion parameters of Cu exposed to the four solutions derived by fitting the EIS data in Figures 3 through 6 with the model in Figure 7(a) are plotted in Figure 8. The plotted parameters are polarization resistance (R$_p$), corrosion rate, double layer capacitance, and solution resistance. The corrosion rate was calculated from R$_p$ using a Stern-Geary constant of 0.027 V/decade, equivalent weight of 64 g, and Cu density of 8.96 g/cm^3, which is the same calculation used by He and Ahn (2017). Figures 8(a) and (b) show that R$_p$ decreased and corrosion rate increased accordingly with increasing chloride concentration from Solution 1 to

8
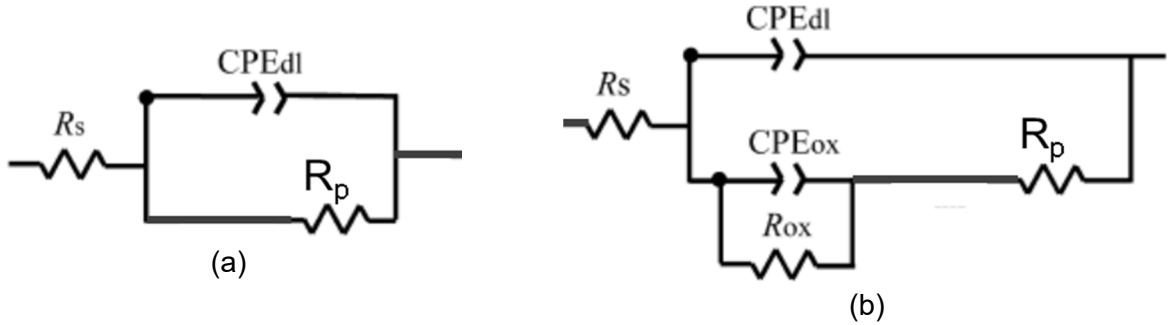
Figure 7. (a) One-time constant and (b) two-time constant circuits used to model the EIS data in Figures 3 through 6 (Rs: solution resistance; Rp: polarization resistance; Rox: oxide resistance; CPEdl: constant phase element of double layer; CPEox: constant phase element of oxide)
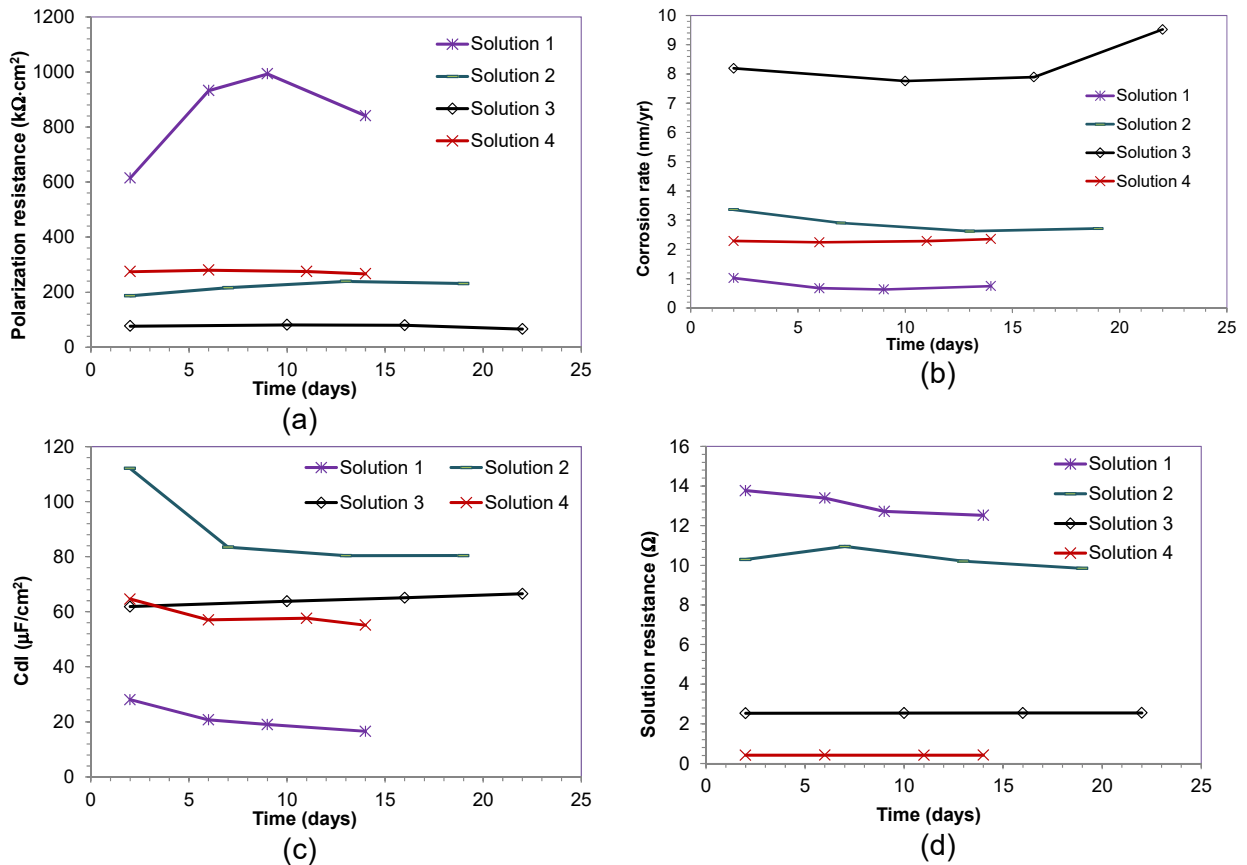
Figure 8. Corrosion parameters of Cu exposed to four solutions derived by fitting the EIS data in Figures 3 through 6 with the model in Figure 7(a): (a) polarization resistance, (b) corrosion rate, (c) double layer capacitance, (d) solution resistance

Solution 3; however, Solution 4 did not follow the trend. The corrosion rate in Solution 4, with the highest chloride concentration, was lower than in Solution 2. This is counter-intuitive as chloride usually enhances corrosion rates of most metals. An exception is King and Watson (2010), who measured the dependence of copper corrosion rates in compacted clay on the salinity of the groundwater and reported that the corrosion rates decreased with increasing Cl^- concentration over the concentration range of 7,100 – 88,750 ppm. At very high Cl^- concentration, the activity of Cl^- may have decreased. Nonetheless, the corrosion rates measured in the current study were all below 10 nm/yr [4×10^{-7} in/yr], which is lower than what was measured by He and Ahn (2017). Possible reasons for the overall lower rates in the current study are: (i) the temperature was lower and (ii) the O_2 concentration in this glovebox was well maintained at an extremely low level, about one order of magnitude lower than that in prior studies (He et al., 2015; He and Ahn, 2017; and He et al. 2018). Figure 8(c) shows that the larger the R_p, the smaller the double layer capacitance. In this case, capacitance depends on the thickness of the double layer and the properties of the dielectric at the interface. As ionic concentration increased from Solution 1 to Solutions 2 and 3, the double layer thickness could have decreased, leading to increasing capacitance. Figure 8(d) shows that, as expected, the solution resistance decreased with increasing chloride concentration.

The electric circuit model in Figure 7(a) indicates that at high frequency, double layer capacitance dominates, but at low frequency, R_p dominates. R_p is directly related to the charge transfer processes associated with corrosion reactions. Figure 9 overlays the 3rd set of EIS data for all four solutions. Comparison of the EIS data in the low frequency region (<0.01 Hz) shows that the electrochemical interface in Solution 4 is dominated by R_p, indicated by near semi-circle behavior in the Nyquist plot and a higher slope of phase angle in the Bode plot. In contrast, the interface in Solution 1 without any Cl^- is dominated by a diffusion process. Overall, the corrosion tendency appears to be negligible in Solution 1 and increased with increasing Cl^- concentration in Solutions 2 through 4.

3.1.3 Corrosion Products

Optical and SEM images of untested and tested Cu electrodes are shown in Figure 10. After the tests, some of the electrodes discolored slightly, but most remained shiny and the same as before the test, even after exposure to Solution 4 with 1×10^5 ppm Cl^-. There are some fractures on the sample surfaces in the SEM images, but fractures also were visible on the untested specimen, suggesting that fractures are artefacts from the silicon carbide (SiC) paper grinding and polishing process used in specimen preparation.

Figure 11 shows the EDX of untested Cu and Cu electrodes after exposure to the four solutions. Table 3 summarizes the untested Cu and posttest Cu surface concentrations of elements detected from EDX. Small amounts of silicon (Si) were present on all the specimens, very likely from the SiC grinding and polishing process for specimen preparation and from glass cell leaching. Sulfur (S) was detected only on Cu exposed to Solution 2 (at 0.37 atomic percent). The lack of S on other test specimens and the small percentage suggests that SO_4^{2-} in all the solutions was not likely involved in the corrosion process. Small amounts of chlorine (Cl) were detected from exposure to Solutions 2 and 3, but not from Solution 4 even though the solution was very concentrated with Cl^-. This suggests that although increasing Cl^- concentration increased the corrosion tendency, detectable corrosion products were not formed because of the low corrosion rate.
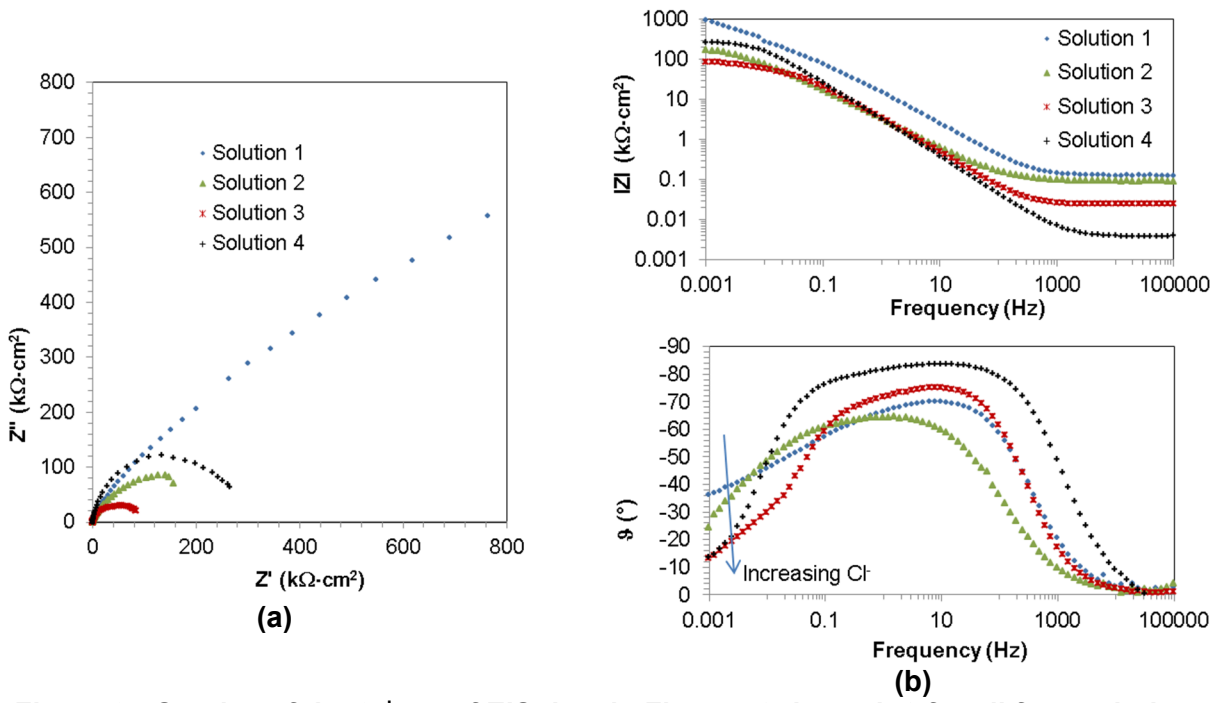
Figure 9. Overlay of the 3rd set of EIS data in Figures 3 through 6 for all four solutions
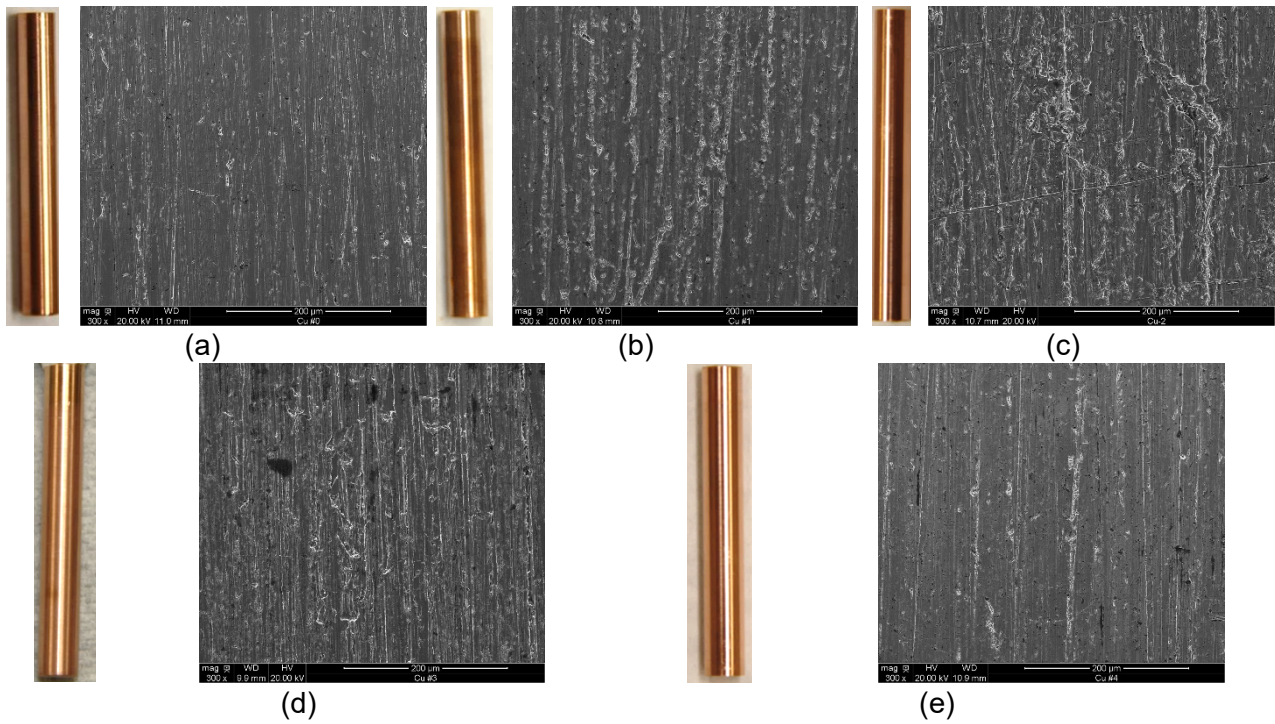

Figure 10. Optical and SEM images of (a) untested Cu and Cu electrodes after exposure to (b) Solution 1, (c) Solution 2, (d) Solution 3, and (e) Solution 4
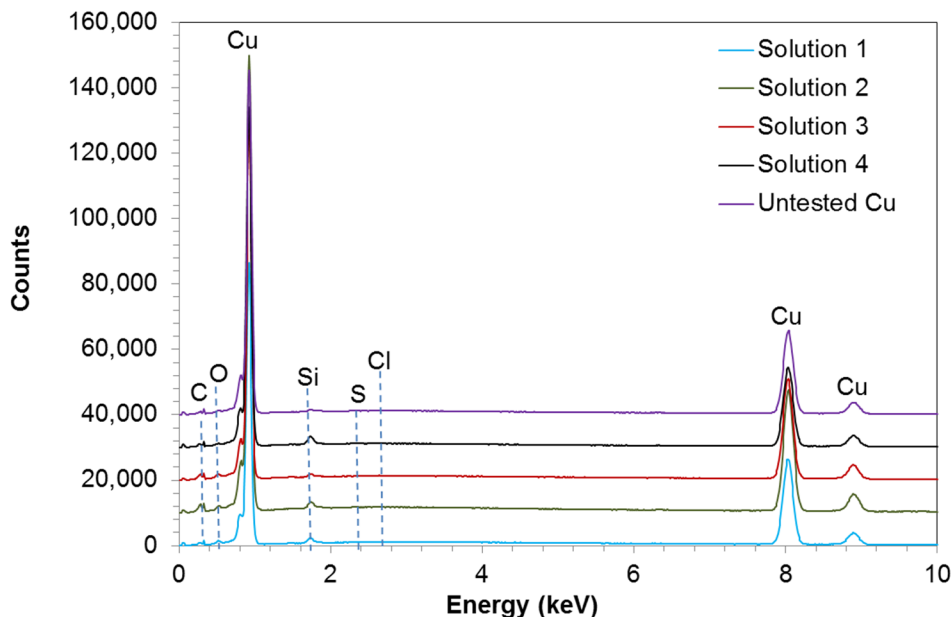
Figure 11. EDX of untested Cu and Cu electrodes after exposure to four solutions

Table 3. Untested Cu and posttest Cu surface concentration of elements detected from EDX					
Elements	**Atomic Percent**				
	Untested Cu	**Solution 1**	**Solution 2**	**Solution 3**	**Solution 4**
Si	1.61	4.36	3.51	1.95	6.88
S	–	–	0.37	–	–
Cl	–	–	0.32	0.65	–
Cu	98.39	95.64	95.80	97.41	92.76

3.2   Cathodic Charging of Carbon Steel in Simulated Concrete Pore Water

The results described in this section correspond to the experiments described in Section 2.2.

Three carbon steel cathodic charging tests were conducted (Table 2). The longest test, which was conducted in a Ca(OH)$_2$ solution, was 3 months long and the other two, conducted in a Ca(OH)$_2$ solution with the addition of 100 ppm Cl$^-$ and SO$_4{}^{2-}$, were only 1.5 months long due to project schedule limitations. Figure 12 shows the cathodic charging potential at an applied charging current of 0.5 mA/cm^2 [3.2 mA/in^2]. The potential needed for the current was in the range of −1.3 to −1.2 V$_{SCE}$ for the first 50 days, but it fluctuated to more cathodic values later on. Figure 13 shows the apex of the posttest carbon steel U-bends. The material was covered by scales that were removed by Clark's solution later. Under microscopic examination, there appears to be a crack on the surface in Figure 13(b). The apex was cross sectioned for confirmation. No crack was observed from other specimens. This suggests that this material is highly resistant to hydrogen induced cracking for the following two reasons: (i) the alkaline solution used in this study forms a passive scale on the material surface, leading to low hydrogen absorption efficiency, and (ii) the short-term static stress on the U-bend does not render cracking susceptibility.
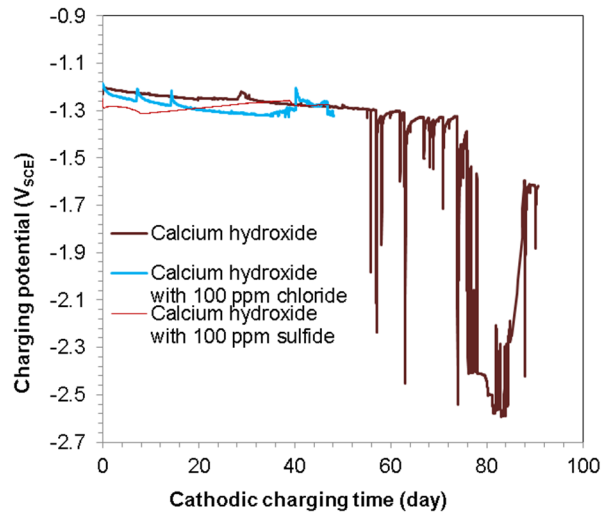
12

**Figure 12. Cathodic charging potential at applying charging current of 0.5 mA/cm²
[3.2 mA/in²] to carbon steel in deaerated simulated concrete pore water at 50 °C [122 °F]**
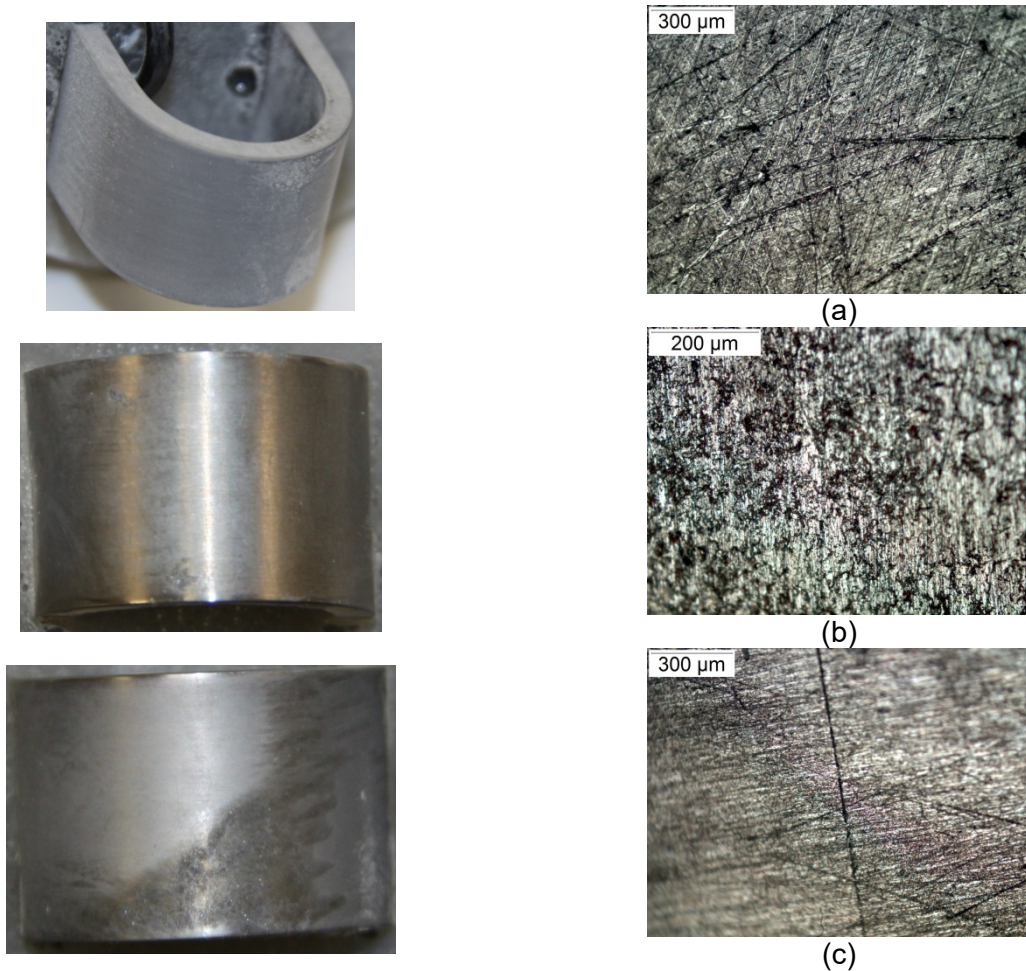
**Figure 13. Posttest carbon steel U-bends exposed to (a) Ca(OH)₂ (b) 100 ppm Cl⁻ and
Ca(OH)₂, and (c) 100 ppm SO₄²⁻ and Ca(OH)₂**

13

4   SUMMARY

4.1   Cu Corrosion

This study investigated the role of Cl^- on Cu corrosion in anaerobic solutions containing SO_4^{2-} and Cl^- only. SO_4^{2-} concentration was kept constant at 2×10^3 ppm, while Cl^- concentration was varied from 0 to 1×10^3, 1×10^4, and 1×10^5 ppm. An anaerobic condition was well maintained in a glovebox purged with N_2. The residual O_2 concentration in the anaerobic solution was about 0.1–0.2 ppb. Electrochemical methods, including open circuit potential monitoring and EIS, were used to study the Cu corrosion properties.

After immersing the electrode in solution, the corrosion potential decreased with time at a faster rate at the beginning, but reached steady state at later times. E_{OC} decreased clearly with increasing Cl^- concentration, leading to a potentially larger corrosion current. All the EIS data in Cl^-–containing solutions showed a mix of resistive and capacitive behavior and the data did not change much with time over the test duration. Diffusion dominated the anodic reaction on the electrode in solution containing SO_4^{2-} only. The commonly accepted one time constant circuit, consisting of polarization resistance, double layer capacitance, and solution resistance, was used to model the EIS data. R_p decreased and corrosion rate increased accordingly with increasing Cl^- concentration from 0, to 1×10^3 ppm, and to 1×10^4 ppm. However, the corrosion rate with 1×10^5 ppm Cl^- was lower than in the solution containing 1×10^3 ppm Cl^-. Nevertheless, all the corrosion rates were below 10 nm/yr [4×10^{-7} in/yr], which is lower than what was measured in our previous work (He and Ahn, 2017). These rates may have been lower because (i) the temperature was lower than in previous tests {20 versus 50 °C [68 versus 122 °F]} and (ii) the O_2 concentration in this glovebox was well maintained at an extremely low level. Overall, comparison of the EIS data suggests that the corrosion tendency was negligible in SO_4^{2-}-only solution and increased with increasing Cl^- concentration. Consistent with the corrosion rates below 10 nm/yr [4×10^{-7} in/yr], there were no noticeable corrosion features observed under a microscope. Although increasing Cl^- concentration increased the corrosion tendency, detectable corrosion products were not formed because of the low corrosion rates. Tests at elevated temperatures are needed to further investigate the roles of Cl^- and other species, such as HCO_3^-, in Cu corrosion.

4.2   Carbon Steel Cathodic Charging

This study investigated the hydrogen induced cracking tendency of carbon steel under cathodic charging in an anaerobic $Ca(OH)_2$ solution used to simulate concrete pore water. A 0.5 mA/cm^2 cathodic charging current was applied to the apex of a U-bend, where the stress was at the maximum. In two of the three tests, 100 ppm Cl^- and 100 ppm S^{2-} were added to the $Ca(OH)_2$ solution. The tests were conducted at 50 °C [122 °F] over 1.5 to 3 months. The potential needed for the current was in the range of −1.3 to −1.2 V_{SCE} for the first 50 days, but it fluctuated to more negative values later on. The posttest material was covered with scales. No cracks were observed on any specimens. The A516 Grade 60 carbon steel material used in this work is highly resistant to hydrogen induced cracking because (i) the alkaline solution forms a passive scale on the surface, leading to low hydrogen absorption efficiency, and (ii) the short-term static stress from the U-bend is not in the range that would render cracking susceptibility. On the other hand, dynamic stress (e.g., straining), such as applied in the work performed by Ahn and Soo (1995), or the formation of thicker scale over a longer time under static stress may break the passive scale. The degradation mechanism of HIC for carbon steel material in

disposal applications will need to be evaluated further under other test conditions, such as dynamic stress.

5 REFERENCES

Ahn, T. and P. Soo. "Corrosion of Low-Carbon Cast Steel in Concentrated Synthetic Groundwater at 80 to 150 °C." *Waste Management*. Vol. 15. pp. 471–476. 1995.

Boyle, C.H. and S.A. Meguid. "Mechanical Performance of Integrally Bonded Copper Coatings for the Long Term Disposal of Used Nuclear Fuel." *Nuclear Engineering and Design*. Vol. 293. pp. 403–412. 2015.

He, X., T. Ahn, J-P. Gwo. "Corrosion of Copper as a Nuclear Waste Container Material in Simulated Anoxic Granitic Groundwater." *Corrosion.* Vol. 74. pp. 158–168. 2018.

He, X. and T. Ahn. "Experiments on Corrosion of Copper and Carbon Steel Waste Containers—Progress Report for Fiscal Years 2015 and 2016." ML17003A453. Washington, DC: U.S. Nuclear Regulatory Commission. 2017.

He, X., T. Ahn, and J. McMurry. "Literature Review and Experiments on Waste Package Corrosion—Copper and Carbon Steel." ML16014A269. Washington, DC: U.S. Nuclear Regulatory Commission. 2015.

King, F. "Container Materials for the Storage and Disposal of Nuclear Waste." *Corrosion*. Vol. 69. pp. 986–1,011. 2013.

King, F. and S. Watson. "Review of the Corrosion Performance of Selected Metals as Canister Materials for UK Spent Fuel and/or HLW." QRA-1384J-1. United Kingdom: Nuclear Decommissioning Authority. 2010.

King, F., M. Kolar, and P.G. Keech. "Simulations of Long-Term Anaerobic Corrosion of Carbon Steel Containers in Canadian Deep Geological Repository." *Corrosion Engineering, Science and Technology*. Vol. 49. pp. 455–459. 2014.

Kursten, B., F. Druyts, D.D. Macdonald, N.R. Smart, R. Gens, L. Wang, E. Weetjens, and J. Govaerts. "Review of Corrosion Studies of Metallic Barrier in Geological Disposal Conditions with Respect to Belgian Supercontainer Concept." *Corrosion Engineering, Science and Technology*. Vol. 46. pp. 91–97. 2011.

Martin, F., S. Perrin, M. Fenart, M. Schlegel, and C. Bataillon. "On Corrosion of Carbon Steels in Callovo-Oxfordian Clay: Complementary EIS, Gravimetric and Structural Study Providing Insights on Long Term Behaviour in French Geological Disposal Conditions." *Corrosion Engineering, Science and Technology*. Vol. 49. pp. 460–466. 2014.

Shibata, T., M. Watanabe, N. Taniguchi, and A. Shimizu. "Modelling of Carbon Steel Corrosion Under Oxygen Depleted Environment." *Corrosion Engineering, Science and Technology*. Vol. 49. pp. 435–441. 2014.

Appendix: Electrochemical Impedance Spectroscopy (EIS)

EIS is an electrochemical method in which an alternating voltage signal is applied to an electrochemical cell and the current response measured. Generally, in a corrosion reaction, both the anodic and cathodic reactions are in their Tafel regions. Thus, a small perturbation, e.g. ± 1–10 mV, about the E_{corr} avoids significant disturbance of the corrosion reaction because the current-potential (I-E) relationship can be taken as linear for a small enough potential perturbation as schematically shown in Figure A-1. For a passive system a similar perturbation can be applied without significantly disturbing the passive state.
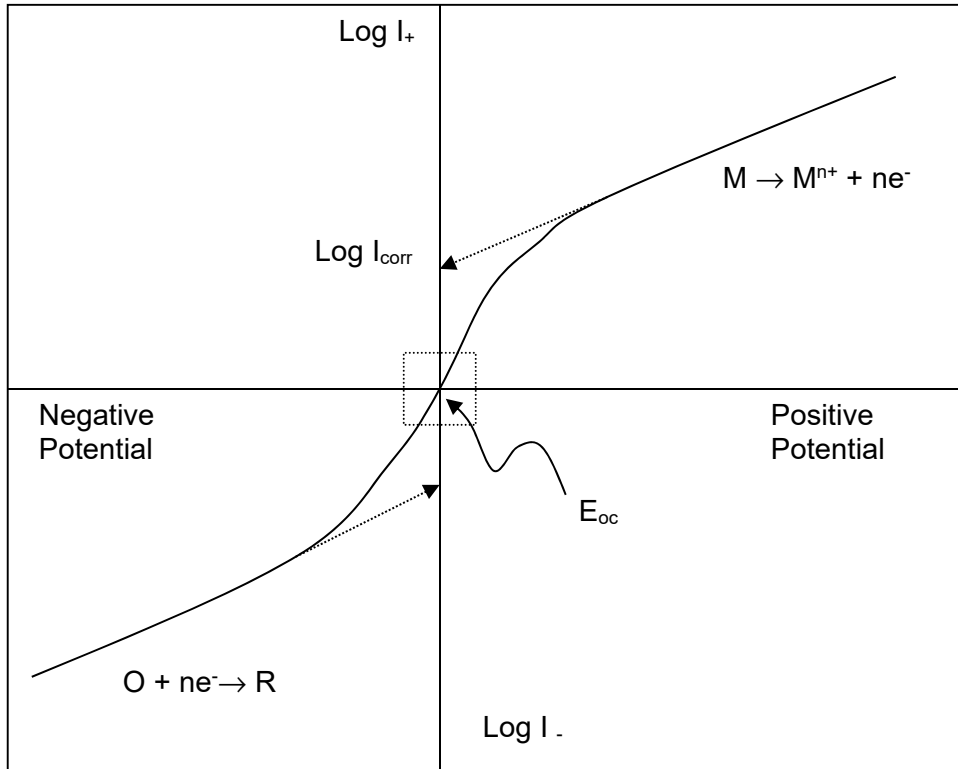

Figure A-1. Current-potential relationship for a corrosion process, showing the separation of the anodic and cathodic half-reactions by polarization to positive and negative potentials, respectively. The box in the Figure signifies the linear region of the polarization curves.

Usually a sinusoidal voltage signal is applied and the resulting current signal is measured. Impedance is the term used to describe the alternating current (AC) equivalent of direct current (DC) resistance. For DC, Ohm's law defines the resistance, R, in terms of the ratio between voltage E and current I:

$$R = E / I \qquad \text{(A-1)}$$

For AC signals, the equivalent parameter is the impedance

$$Z = E / I \qquad \text{(A-2)}$$

However, the impedance of a circuit depends on the frequency of the applied signals. In a linear (or pseudo-linear) system, the current response to a sinusoidal potential will be a sinusoid at the same frequency but shifted in phase, as shown in Figure A-2. If the applied signal, expressed as a function of time, has the form

$$E(t) = E_0\ sin(\omega t) \qquad \text{(A-3)}$$

where $E(t)$ is the potential at time t, E_0 is the amplitude of the signal, and ω is the angular frequency of the sine wave, then the resulting current signal will be

$$I(t) = I_0\ sin(\omega t + \varphi) \qquad \text{(A-4)}$$

where φ is the phase shift as indicated in Figure A-2.
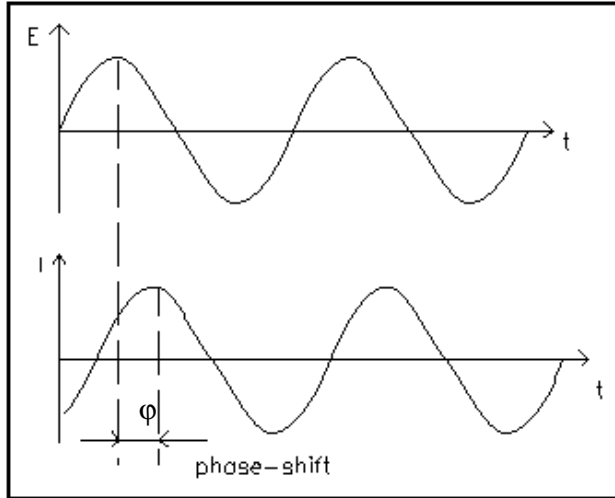
The impedance Z can then be calculated as:

Figure A-2. Sinusoidal current response to a sinusoidal potential input in a linear system showing the phase-shift between the input and output signals.

$$Z = \frac{E(t)}{I(t)} = \frac{E_0 \sin(\omega t)}{I_0 \sin(\omega t + \varphi)} = Z_0 \frac{\sin(\omega t)}{\sin(\omega t + \varphi)} \qquad \text{(A-5)}$$

Mathematically, the impedance can also be represented in terms of real and imaginary components as,

$$Z = Z' + j\ Z'' \qquad \text{(A-6)}$$

where Z' and Z'' are the real (in-phase) and imaginary (out of phase) components of the impedance.

So the impedance of a system at a given frequency can be calculated based on the amplitudes of the input AC voltage signal, the output AC signal and the phase angle (proportional to the

18

shift in time between peak current and peak voltage). The actual measuring equipment processes the current-time and the voltage-time measurements to yield the impedance at different frequencies, which provides an impedance spectrum. The spectrum is often plotted in two forms. If the real part is plotted on the *X-axis* and the imaginary part on the *Y-axis* of a chart, this is named a Nyquist plot. If both the absolute value of the impedance ($|Z| = Z_0$) and phase angle are plotted against log (frequency), this presentation method is termed a Bode plot. Unlike the Nyquist plot, the Bode plot shows the frequency information for the whole frequency range.

EIS data are commonly analyzed by fitting them to an equivalent electrical circuit model (EECM), such as the simple circuit shown in Figure A-3(a). This circuit is commonly used to represent the behaviour of a metal electrode in solution consisting of a solution resistance (R_s), polarization resistance (R_p), and double layer capacitance (C_{dl}). A system that has both resistive and capacitive attributes can be described as having a time constant, τ, which is the product of the measured resistance and the capacitance ($\tau = RC$). The impedance of the circuit is in following equation:

$$Z = R_s + (\frac{1}{R_p} + j\omega C_{dl})^{-1} \qquad \text{(A-7)}$$
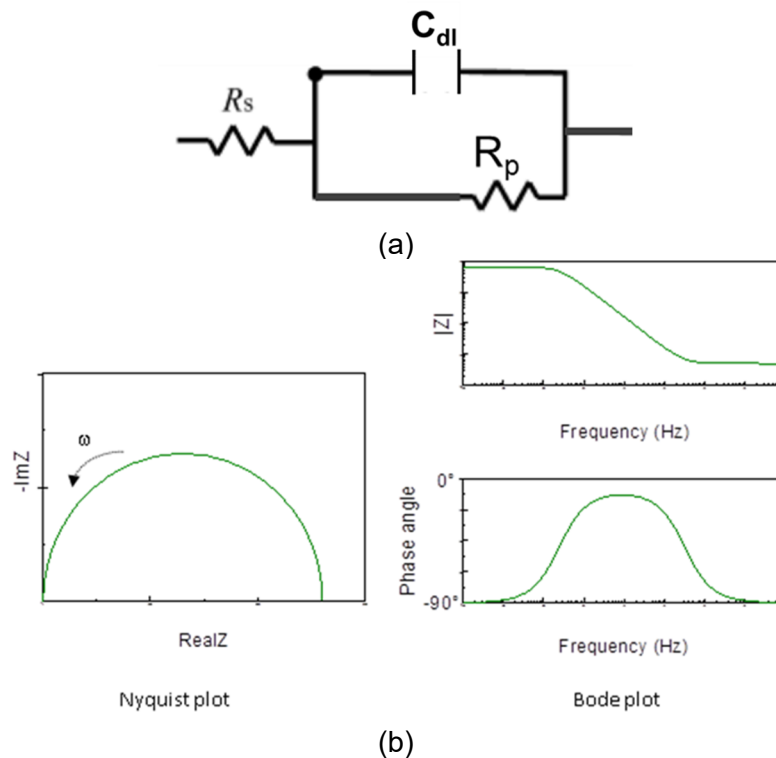

(a)

(b)

Figure A-3. (a) Representation of a simple equivalent circuit with one time constant consisting of a solution resistance (R_s), polarization resistance (R_P), and double layer capacitance (C_{dl}), (b) Nyquist plot and Bode plot for the one time constant circuit in (a).

The impedance spectrum for a real system generally contains more circuit elements leading to a more complex behaviour. Most of the circuit elements in the model are common electrical elements, such as resistors, capacitors, and inductors. The impedance of a resistor is independent of frequency with only a real component; consequently the current through a resistor is always in phase with the voltage. In contrast, capacitors have only an imaginary

impedance component, and the current through a capacitor is phase shifted –90 degrees with respect to the voltage. Figure A-3(b) shows schematically the frequency response of the simple circuit in Figure A-3(a) per Equation (A-7), where the phase shift of –90 degrees is shown. At high frequency, resistance of C_{dl} is low. Current predominantly flows through R_s and C_{dl}. At low frequency, resistance of C_{dl} is high. Current predominantly flows through R_s and R_p.

Figure A-4(a) is representation of an equivalent circuit with two time constants consisting of a solution resistance (R_s), oxide film resistance (R_{ox}), oxide film capacitance (C_{ox}), polarization resistance (R_P), and double layer capacitance (C_{dl}). The impedance of Figure A-4(a) is described in Equation (A-8). Figure A-4(b) is Nyquist plot and Bode plot for the two time constants circuit in Figure A-4(a) per Equation (A-8). Two semicircles in the Nyquist plot, two peaks in the phase angle, and two plateaus in the impedance amplitude in the Bode plot correspond to the two time constants in the circuit. The separation of the peaks, plateaus, and semicircles depends on the difference between C_{dl} and C_{ox}, R_{ox} and R_P. In actual electrochemical system, these features are mostly not clearly separated. Computer program is used to deconvolute the circuit elements.

$$Z = R_s + \left(\cfrac{1}{R_p + (j\omega C_{ox} + \cfrac{1}{R_{ox}})^{-1}} + j\omega C_{dl} \right)^{-1} \tag{A-8}$$
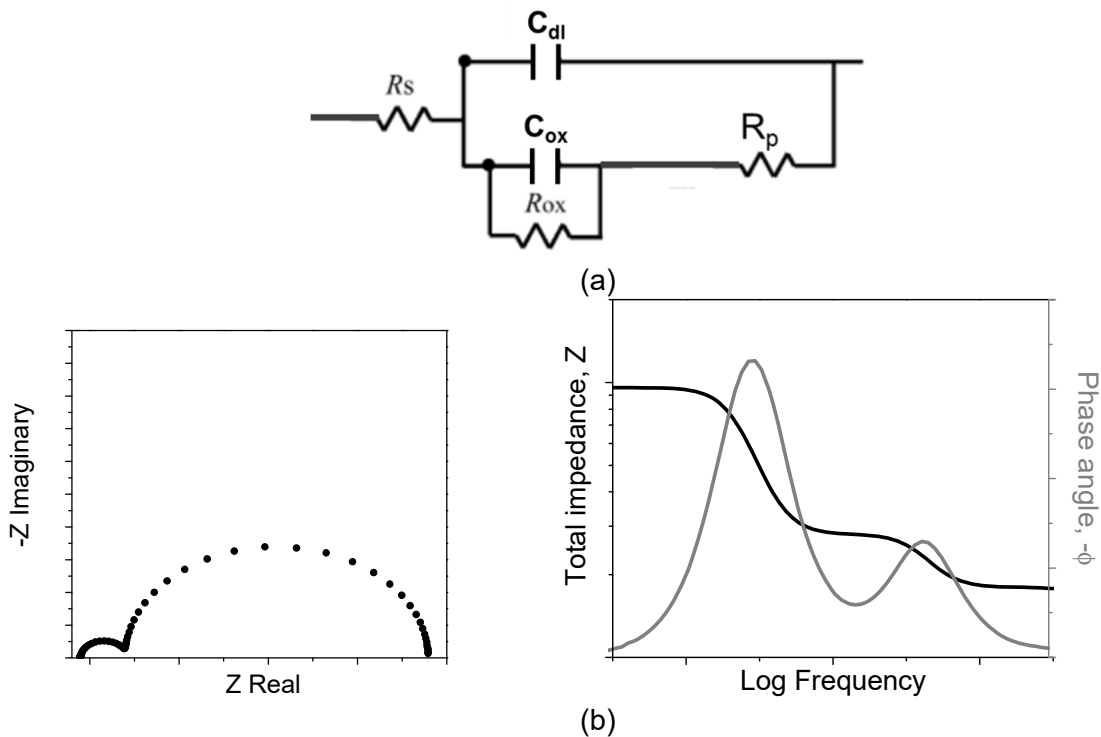

(a)

(b)

Figure A-4. (a) Representation of an equivalent circuit with two time constants consisting of a solution resistance (R_s), oxide film resistance (R_{ox}), oxide film capacitance (C_{oxide}), polarization resistance (R_P), and double layer capacitance (C_{dl}) (b) Nyquist plot and Bode plot for the two time constants circuit in (a).

The type of electrical components comprising the EECM and their interconnections affect the fit of the model to the measured EIS spectrum. To be meaningful, the elements in the model must represent a physical electrochemical basis of the system; for example, most models contain a resistor that models solution resistance between the two electrodes in the cell. Capacitors in EIS experiments often do not behave ideally. For example, the double layer usually does not behave ideally as a capacitor as shown in Figure A-3(a) because usually the thickness is not uniform on the metal electrode. Instead, constant phase elements (CPE) are often used to replace ideal capacitors to compensate for non-homogeneity in the system. Formally, the impedance of a CPE is given by

$$Z = Z_0(j\omega)^{-n} \qquad\qquad\qquad\text{(A-9)}$$

If $n = 0$, then the CPE is a resistor with $R = Z_0$. If $n = 1$ the CPE is a capacitor with $C = 1/Z_0$. The CPE is, in fact, a general combination for many circuit elements and n is between 0 to 1.

Diffusion processes also yield a frequency response and can be represented by a Warburg diffusion element. A Warburg impedance (Z_W) element can be used to model semi-infinite linear diffusion; that is, unrestricted diffusion to a large planar electrode. This impedance depends on the frequency of the potential perturbation and is inversely proportional to the square root of the frequency as in following equation

$$Z_W = \sigma\omega^{1/2}(1\text{-}j) \qquad\qquad\text{(A-9)}$$

The Warburg is unique among CPE's because the real and imaginary components are equal at all frequencies and both depend upon $1/\omega^{1/2}$. On a Nyquist plot, the Warburg impedance is observed as a straight line with a slope of 45°. On Bode plots the Warburg impedance is observed at low frequencies, and exhibits a phase shift of 45° in the phase angle plot and appears as a straight line with a slope around 0.5 (in between capacitive and resistive behavior) in the impedance magnitude plot.
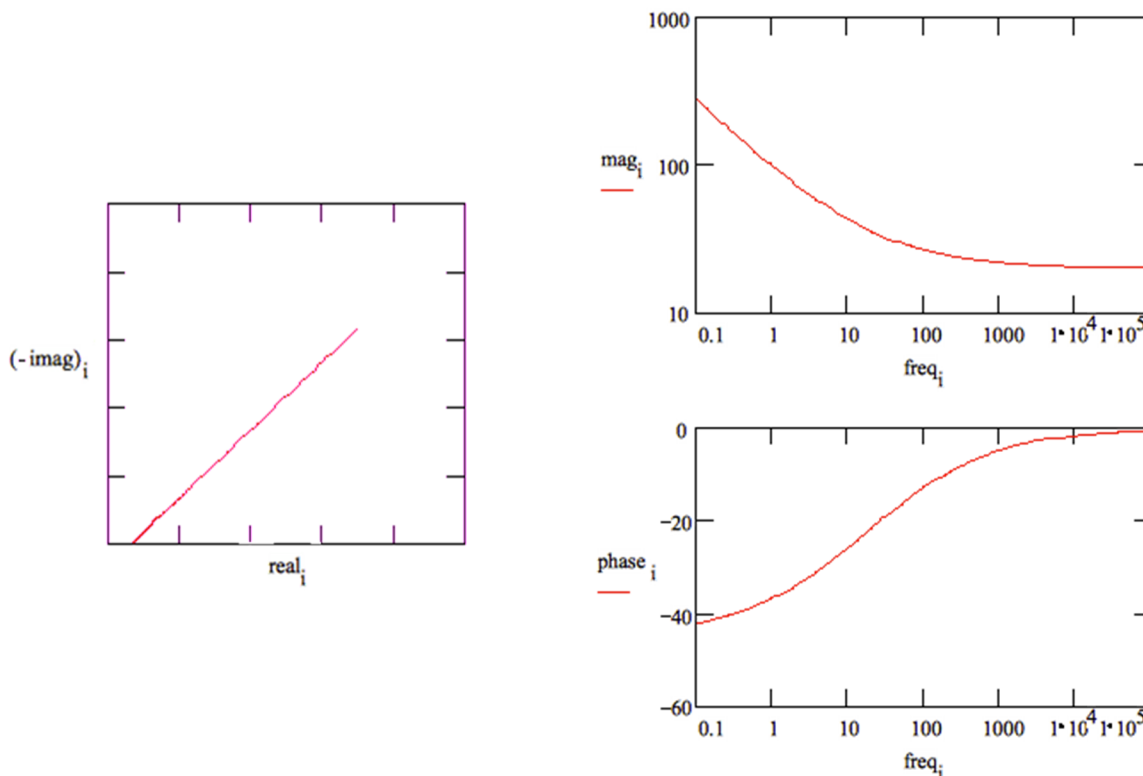
Figure A-5. Nyquist and Bode plots for Warburg impedance

EIS is a powerful technique for investigating electrochemistry and corrosion systems. It can be used to determine interfacial parameters, such as reaction rates, rate constants, interfacial capacitances, and to study reaction mechanisms and to investigate materials properties, such as film resistance, electrical permittivity, dielectric constants, and film thickness. However, EIS data obtained from fitting to an equivalent circuit must be treated with caution, since there is no unique equivalent circuit and set of parameter values that describe the spectrum. It cannot be assumed that an equivalent circuit that produces a good fit to a data set necessarily represents an accurate physical model of the cell. Empirical models should use the fewest elements possible and other methods should be used to supplement EIS data. More details on the theoretical basis and applications can be found in the literature (Bard and Faulkner, 2001; Cottis and Turgoos, 1999; Macdonald, 1989).

References

Bard, A.J., L.R. Faulkner. "Electrochemical Methods, Fundamentals and Applications." 2nd edition. John Wiley & Sons, Inc., New York. 2001.

Cottis, R.. S. Turgoos. "Electrochemical Impedance and Noise." NACE International, USA, 1999.

Macdonald, D.D.. "Electrochemical Impedance Spectroscopy." in Electrochemical and Optical Techniques for the Study and Monitoring of Metallic Corrosion., M.G.S. Ferreira and C.A. Melendres, eds., Kluwer Academic Publishers, Dordrecht, Netherlands, 1989.